

Viscous QCD matter in a hybrid hydrodynamic+Boltzmann approach

Huichao Song,^{1,2,*} Steffen A. Bass,³ and Ulrich Heinz²

¹*Nuclear Science Division, Lawrence Berkeley National Laboratory, Berkeley, California 94720, USA*

²*Department of Physics, The Ohio State University, Columbus, Ohio 43210, USA*

³*Department of Physics, Duke University, Durham, North Carolina 27708, USA*

(Dated: May 23, 2018)

A hybrid transport approach for the bulk evolution of viscous QCD matter produced in ultra-relativistic heavy-ion collisions is presented. The expansion of the dense deconfined phase of the reaction is modeled with viscous hydrodynamics while the dilute late hadron gas stage is described microscopically by the Boltzmann equation. The advantages of such a hybrid approach lie in the improved capability of handling large dissipative corrections in the late dilute phase of the reaction, including a realistic treatment of the non-equilibrium hadronic chemistry and kinetic freeze-out. By varying the switching temperature at which the hydrodynamic output is converted to particles for further propagation with the Boltzmann cascade we test the ability of the macroscopic hydrodynamic approach to emulate the microscopic evolution during the hadronic stage and extract the temperature dependence of the effective shear viscosity of the hadron resonance gas produced in the collision. We find that the extracted values depend on the prior hydrodynamic history and hence do not represent fundamental transport properties of the hadron resonance gas. We conclude that viscous fluid dynamics does not provide a faithful description of hadron resonance gas dynamics with predictive power, and that both components of the hybrid approach are needed for a quantitative description of the fireball expansion and its freeze-out.

PACS numbers: 25.75.-q, 12.38.Mh, 25.75.Ld, 24.10.Nz

I. INTRODUCTION

The discovery that ultrarelativistic heavy-ion collisions at the Relativistic Heavy-Ion Collider (RHIC) produce dense, color deconfined matter that thermalizes quickly into a quark-gluon plasma (QGP) [1] and subsequently evolves like an almost perfect liquid [2–5] with near-minimal viscosity [6, 7] has generated intense interest in a quantitative determination of the QGP transport properties [8–12]. Since the QGP liquid stage is sandwiched between an early pre-equilibrium and a final hadronic rescattering and decoupling stage, both of which have different transport properties, such a determination requires a complete dynamical description of all stages of the fireball expansion [11]. Stated differently, when one uses experimental observables that are sensitive to the transport properties of the expanding medium (for example, the elliptic flow v_2 has been shown to be particularly sensitive to shear viscosity [8–13]), contributions from the pre-equilibrium and hadronic freeze-out stages to these observables must be accurately known for a precise determination of the QGP transport coefficients. Purely hydrodynamic calculations, that substitute hydrodynamic initial conditions for a full dynamical solution of the pre-equilibrium stage and replace the kinetic hadron freeze-out process by a sudden transition from thermalized fluid to non-interacting particles using the Cooper-Frye prescription [14], require additional parameters whose values may influence the extracted thermal and transport properties, and they will always be

plagued by irreducible systematic uncertainties in the extracted values that result from the crude modeling of the early and late non-equilibrium stages.

This insight is not new, and it has spurred the development of hybrid algorithms that describe different stages of the expansion with different tools for the last ten years. The main advantage of a hydrodynamic description (where valid) over kinetic theory is its relative simplicity: only a few macroscopic fields (energy and baryon density, pressure and flow velocity) must be evolved in space-time, whereas the microscopic approach requires to follow the evolution of both the momenta and positions of all particles. The phenomenological success of hydrodynamic modeling for heavy-ion collisions thus leads naturally to the concept of using a fluid dynamical description as the backbone of the complete evolution model, interfaced with computationally more demanding microscopic algorithms to describe the early and late non-equilibrium stages. For the hadronic rescattering phase several microscopic algorithms that solve coupled Boltzmann equations for the hadron distribution functions were developed and extensively tested in the 1980s and '90s [15–19]. Hybrid codes that coupled an ideal fluid dynamical description of an expanding QGP to such hadronic rescattering codes and compared the results with purely fluid dynamical calculations began to appear about ten years ago [20–23]. Here we present the first hybrid model that interfaces *viscous* relativistic hydrodynamics (specifically the (2+1)-dimensional algorithm VISH2+1 [10]) with a hadronic Boltzmann cascade (specifically the Monte Carlo algorithm UrQMD [18]), via the “hydro-to-OSCAR” converter H₂O that converts hydrodynamic output into hadrons, with positions and mo-

* Correspond to HSong@lbl.gov

menta given in OSCAR format¹ that can be read by UrQMD. We call this hybrid code VISHNU.² In the present version of VISHNU the pre-equilibrium stage is not yet described dynamically, but continues to be replaced by initial conditions for the fluid dynamic evolution.

An essential ingredient in VISHNU is the use of a state-of-the-art equation of state (EOS) for hot QCD matter, s95p-PCE [24, 25], which incorporates our best knowledge of the relation between pressure, energy and entropy density in the deconfined QGP stage from Lattice QCD [26] (see also [27]) and matches it to a realistic hadron resonance gas (HRG) at low temperatures, taking into account that the abundances of stable hadrons (after strong decays of unstable resonances) are experimentally known to freeze out at $T_{\text{chem}} \approx 165$ MeV [28]. This requires the introduction of properly adjusted, temperature dependent non-equilibrium chemical potentials for all hadronic species below T_{chem} [31–34]. Chemical freeze-out is immediate³ and automatic in UrQMD, due to the rapid three-dimensional expansion of the fireball in the hadronic stage [29]. This implies that the hydrodynamic output that is fed into UrQMD must have the correct chemical composition, since otherwise the final hadron abundances disagree with experiment. If we decrease the switching temperature T_{sw} for the transition from hydrodynamics to hadron cascade below the chemical freeze-out temperature T_{chem} , the hydrodynamic output thus has to reflect the correct partial chemical equilibrium (PCE) abundances that would, after resonance decays, produce the correct final yield ratios. This is also important for the elliptic flow: Although the non-equilibrium chemical potentials have a very small effect on the equation of state $p(e)$ [32], the distribution of the total momentum anisotropy among hadron species strongly depends on the chemical composition of the hadronic system [32–35]. A comparison between chemical equilibrium and partial chemical equilibrium EOS in ideal hydrodynamics shows that the breaking of chemical equilibrium in the HRG can increase the differential elliptic flow $v_2(p_T)$ for pions by 25% [32, 34].

VISHNU was developed to remove uncertainties from non-equilibrium dynamics during the late hadronic stage when extracting QGP transport coefficients from experimentally measured final hadron spectra. The main goals of the present article, however, are purely conceptual: by comparing the hadron spectra and differential elliptic flow from VISHNU with those from purely hydrodynamic simulations with different (temperature dependent) values for the shear viscosity to entropy density ratio η/s

during the HRG stage, we want to establish to what extent the microscopic UrQMD dynamics of the HRG phase can be mimicked by an effective macroscopic calculation based on viscous fluid dynamics. By varying the switching temperature between VISH2+1 and UrQMD we explore the existence of a “switching window”, i.e. of a range of temperatures within which both VISH2+1 (with an appropriate choice of transport coefficients) and UrQMD provide a valid description of the fireball evolution. Our goal here is *not* to compare VISHNU with experimental data from RHIC; this is done elsewhere [12]. Consequently, we explore the sensitivity of our results to variations in the hydrodynamic initial conditions only to the extent that they affect the answer to the above questions.

The paper is organized as follows. In Sec. II we briefly present the three components of VISHNU: the viscous hydrodynamic algorithm VISH2+1, the hydro-to-micro converter H₂O, and the hadron cascade UrQMD. In Sec. III we compare basic observables (spectra and elliptic flow) from VISHNU and pure viscous hydrodynamics, using both chemical equilibrium and PCE equations of state as input. In Sec. IV we test the switching temperature dependence of the final spectra and elliptic flow obtained with VISHNU, extracting an effective viscosity $(\eta/s)(T)$ for UrQMD under dynamical conditions provided by RHIC collisions. We interpret our findings and summarize our results in Sec. V. Appendix A describes tests of the hydro-to-micro converter H₂O and shows some results that demonstrate its accuracy.

II. VISHNU: COUPLING VISCOUS HYDRODYNAMICS TO A HADRON CASCADE

In this section we describe the structure of VISHNU, a hybrid code that couples the viscous hydrodynamic expansion of the QGP stage in heavy-ion collisions to a microscopic kinetic evolution of the dilute late hadronic stage using a Boltzmann Monte Carlo approach. The hydrodynamic component allows for ideal fluid evolution in the limit of zero transport coefficients. We here include only shear viscosity, neglecting bulk viscous contributions from the QGP and hadronization stages whose effects on spectra and elliptic flow are expected to be small [36, 37].⁴ We assume zero net baryon density everywhere and thus do not follow explicitly the evolution of the baryon current. The latter can be easily included in future versions of the code.

The viscous hydrodynamic and microscopic kinetic algorithms are interfaced with each other through the Monte Carlo event generator H₂O that converts hydrodynamic output on a hypersurface of constant temperature T_{sw} to particles, by sampling the corresponding

¹ <http://karman.physics.purdue.edu/OSCAR-old/>

² “Viscous Israel-Stewart Hydrodynamics aNd UrQMD”.

³ It is a consequence of the smallness of particle-changing inelastic cross sections when compared with the much larger elastic and (resonance dominated) quasielastic scattering cross sections that keep the hadron gas close to thermal (but not chemical) equilibrium for a range of temperatures below T_{chem} [30].

⁴ Bulk viscous effects from the hadron resonance gas stage [38] are automatically accounted for by the Boltzmann cascade component of the hybrid code.

Cooper-Frye [14] phase-space distributions, including viscous corrections. This procedure requires switching temperatures T_{sw} that are low enough for UrQMD to provide a reliable description of the subsequent hadronic rescattering dynamics. The highest possible switching temperature is therefore $T_{\text{sw}} = T_c$ where T_c denotes the (pseudo)critical temperature for the quark-hadron phase transition. Higher T_{sw} values would require a microscopic description of the hadronization process itself, including accompanying changes in vacuum structure, and knowledge of the effective particle degrees of freedom during this process. This is at present an unsolved problem.

For comparison we also perform purely hydrodynamic simulations without the hadronic cascade, by running VISH2+1 to lower temperatures and decoupling directly into free-streaming particles, by using the Cooper-Frye prescription at T_{dec} . These comparison runs are done with constant or temperature-dependent specific shear viscosities η/s in the hadronic phase. For the QGP phase we use constant η/s , motivated the weak (logarithmic) temperature dependence of η/s predicted by perturbative QCD in the weak-coupling limit [39] and the temperature independence of η/s predicted by the AdS/CFT correspondence in the strong coupling limit [7].⁵

In the following subsections we discuss the components of VISHNU in more detail.

A. Viscous hydrodynamics (VISH2+1)

For the hydrodynamic stage we use VISH2+1, a (2+1)-dimensional viscous hydrodynamic code with longitudinal boost invariance [10]. The specific implementation used in the present work, including the equation of state s95p-PCE, is described in Sections II and III of Ref. [25] to which we refer the reader for technical details. For later reference we note that the relaxation time for the shear pressure tensor is set to $\tau_\pi = 3\eta/(sT)$. In some of the comparison runs we also employ the equation of state SM-EOS Q described in [10] which assumes a first-order quark-hadron phase transition and chemical equilibrium (CE) in the hadronic phase. The comparison between pure hydrodynamic simulations with s95p-PCE and SM-EOS Q (CE) emphasizes the effects arising from the breaking of chemical equilibrium in the hadronic phase at temperatures below $T_{\text{chem}} = 165$ MeV.

Different from Ref. [25], we here use as default initial conditions an initial energy density profile taken to be 100% proportional to the wounded nucleon density

from the optical Glauber model whose peak energy density in central ($b=0$) Au+Au collisions is normalized to $e_0 \equiv e(r=0, \tau_0; b=0) = 30 \text{ GeV}/\text{fm}^3$, with $\tau_0 = 0.6 \text{ fm}/c$. This gives roughly the correct final charged hadron multiplicity dN_{ch}/dy in central collisions, but does not correctly reproduce its measured nonlinear dependence on the total number of wounded nucleons N_{part} in noncentral collisions. For the purposes of the present conceptual study this is not essential.

In Sec. IV, in order to test the “universality” of the effective temperature-dependent $(\eta/s)(T)$ for UrQMD extracted by comparing VISHNU with VISH2+1, we also use Color Glass Condensate (CGC) motivated initial conditions, obtained by averaging a large number of fluctuating initial entropy density profiles computed with the fKLN Monte Carlo code⁶ [40] after recentering them and aligning their major axes.⁷ The resulting smooth average entropy density is converted to an initial energy density profile using the EOS. This procedure accounts, in an average way, for event-by-event fluctuations in the initial source eccentricity, giving (depending on impact parameter) $\sim 30 - 100\%$ larger initial eccentricities than the optical Glauber model (see [41] for details). For both optical Glauber and fluctuating fKLN initial profiles we assume zero transverse flow at the beginning of the hydrodynamic evolution at τ_0 .

B. Hydro-to-micro converter (H_2O)

To convert the hydrodynamic output into particles that can then be further propagated with the hadron cascade UrQMD we first use the AZHYDRO algorithm to find an isothermal freeze-out surface $\Sigma(x)$ of temperature T_{sw} and then calculate the hadron spectra with the Cooper-Frye formula [14] (see [10] for details). H_2O is a Monte Carlo event generator that samples tiles on Σ and generates the position x and momentum p of a particle of species i with a probability derived from the differential Cooper-Frye formula:

$$\begin{aligned} E \frac{d^3 N_i}{d^3 p}(x) &= \frac{g_i}{(2\pi)^3} p \cdot d^3 \sigma(x) f_i(x, p) \\ &= \frac{g_i}{(2\pi)^3} p \cdot d^3 \sigma(x) [f_{\text{eq},i}(x, p) + \delta f_i(x, p)]. \end{aligned} \quad (1)$$

Here g_i is the degeneracy factor for hadron species i , and $d^3 \sigma_\mu(x)$ is the outward-pointing surface normal vector of the selected tile at point x on the surface Σ . $f_i(x, p) = f_{\text{eq},i}(x, p) + \delta f_i(x, p)$ is the local distribution function for hadron species i , consisting of a local equi-

⁵ We acknowledge that near T_c QCD is not a conformal field theory and that therefore in the temperature region accessible at RHIC ($T_c \leq T \lesssim 2T_c$) η/s might very well feature a stronger temperature dependence than predicted by both perturbative QCD and the strong coupling limit for conformal field theories. Heavy-ion experiments at the LHC are expected to shed light on this question.

⁶ Available at URL [http://th.physik.uni-frankfurt.de/~drescher/CGC/]

⁷ The CGC initial profiles were provided by T. Hirano [41]. The same profiles were used in [12].

librium part (here with $\mu = 0$)

$$f_{\text{eq},i}(x, p) = \frac{1}{e^{p \cdot u(x)/T(x)} \pm 1} \quad (2)$$

and a (small) deviation δf_i from local equilibrium due to shear viscous effects. For δf we make the quadratic ansatz (see [8, 42] for a discussion of this and other possibilities)

$$\delta f(x, p) = f_{\text{eq}}(p, x) (1 \mp f_{\text{eq}}(p, x)) \frac{p^\mu p^\nu \pi_{\mu\nu}(x)}{2T^2(x) (e(x) + p(x))} \quad (3)$$

(the upper (lower) sign is for fermions (bosons)). δf is proportional to the shear viscous pressure tensor $\pi^{\mu\nu}(x)$ on the freeze-out surface and increases (in our case) quadratically with the particle momentum. In the limit $\eta/s \rightarrow 0$ (i.e. for ideal fluid dynamics) δf vanishes.

Since VISH2+1 is a (2+1)-dimensional code with longitudinal boost invariance but UrQMD propagates particles in all three spatial dimensions, we extend the VISH2+1 output analytically from midrapidity ($y=0$) to non-zero momentum rapidities, using boost invariance. After having determined the transverse position and transverse momentum of a particle using a space-time rapidity integrated version of Eq. (1) as weight, we sample its momentum rapidity y randomly within the finite range $-3 < y < 3$, with a sharp cutoff at its upper and lower ends. (We restricted the range to $|y| < 3$ to minimize the excitation of strings in UrQMD.) Its space-time rapidity η_s (defining its longitudinal position) is then sampled according to the η_s -dependence of Eq. (1) (see Eq. (A1) for an explicit expression). This results in an η_s distribution of the generated particles that is flat near $\eta_s = 0$ but smeared at the edges around $\eta_s = \pm 3$ (see inset in Fig. 15 for illustration). UrQMD propagates the resulting particles in all three spatial directions but (due to the nearly boost-invariant input over the y - and η_s -range mentioned) preserves boost invariance of the final momentum distributions accurately within the region $|y| < 1.5$. This allows comparison of the calculations with midrapidity data from the RHIC experiments without having to worry about edge effects from the rapidity cut-off in H₂O.

The default switching temperatures used in this article are $T_{\text{sw}} = 165$ MeV for s95p-PCE and $T_{\text{sw}} = 160$ MeV for SM-EOS Q (CE). Here, 165 MeV is equal to the chemical freeze-out temperature T_{chem} used in s95p-PCE, and 160 MeV is the transition temperature from the mixed to hadronic phase in SM-EOS Q [10]. In Sec. IV we also use lower T_{sw} values in order to study the existence of a switching window for VISHNU.

For each hydrodynamic run we use H₂O to generate a large number of events⁸ whose particles are then fur-

ther propagated with UrQMD until all collisions cease and unstable resonances have decayed. In the purely hydrodynamic simulations we run the converter on the final decoupling surface with temperature T_{dec} to generate events of free-streaming hadrons with similar statistics. (We use $T_{\text{dec}} = 100$ MeV with EOS s95p-PCE and $T_{\text{dec}} = 130$ MeV with SM-EOS Q (CE), corresponding to similar decoupling energy densities [32].) In these runs we have no further hadronic collisions and only allow the unstable resonances to decay, and analyze the final state with the same tools as used for complete VISHNU runs.

C. Microscopic hadronic transport (UrQMD)

For the modeling of the hadronic phase, we use the Ultra-relativistic Quantum Molecular Dynamics (UrQMD) model [18], a microscopic hadronic transport model based on the Boltzmann equation. UrQMD, which was initially developed as an ab-initio model for the simulation of relativistic heavy-ion collisions, is well suited for the description of a hadron gas in and out of chemical equilibrium [30, 43–45] and has been successfully applied to previous hybrid micro+macro transport approaches based on ideal fluid dynamics [20, 23, 46].

In UrQMD, the system evolves through a sequence of binary collisions and $2 \rightarrow N$ decays of mesons and baryons. The cross sections are assumed to be free vacuum cross sections and depend on the center of mass energy of the two colliding hadrons as well as on their flavor and quantum numbers. The UrQMD collision term contains 49 different baryon species (including nucleon, delta and hyperon resonances with masses up to 2 GeV) and 25 different meson species (including strange meson resonances), which are supplemented by their corresponding anti-particle and all isospin-projected states. Full baryon/antibaryon symmetry is included. For excitations with higher masses a string picture is used. All states listed can be produced in string decays, s-channel collisions or resonance decays.

Tabulated or parameterized experimental cross sections are used when available, resonance absorption and scattering is handled via the principle of detailed balance. If no experimental information is available, the cross section is either calculated via an OBE model or via a modified additive quark model which takes basic phase space properties into account. A detailed overview of the elementary cross sections and processes included in the UrQMD model is given elsewhere [18].

When modeling the hadronic phase subsequent to the decay of a thermalized QGP, we find that the relative momenta and c.m. energies of the individual hadron-hadron interactions are rather small and therefore string excitations and decays are strongly suppressed and occur rarely. The dominant forms of interactions encountered are elastic scattering and inelastic scattering through resonance formation and decay.

It is important to note that UrQMD makes no equilib-

⁸ Sufficient accuracy for the p_T -integrated v_2 is obtained with event samples ranging from 2,000 for 0-5% centrality to 72,000 for 70-80% centrality. For Figs. 1–3 we used 90,000 events in order to obtain sufficient statistics for $v_2(p_T)$ of protons out to $p_T = 2$ GeV/ c .

rium assumptions and can therefore be utilized for the description of systems in and out of equilibrium. **UrQMD** will retain equilibrium if given an equilibrium initial condition with suitable boundary conditions. This characteristic allows for the construction of our hybrid approach, since it ensures that **UrQMD**'s response to the microscopic hadronic configuration generated by H_2O will initially mimic the response of the viscous hydrodynamic model. However, the real advantage of transitioning to a microscopic transport such as **UrQMD** lies in its ability to describe the evolution of systems out of equilibrium, e.g. prior to equilibration or during the break-up and freeze-out stage of the reaction when assumptions of chemical and/or kinetic equilibrium are no longer valid.

By virtue of its microscopic nature, **UrQMD** takes the full local temperature and particle fugacity dependence of the hadronic viscosity into account [45], even though it may be challenging to quantify the exact value of the hadronic viscosity inherent in the **UrQMD** calculation of the hadronic phase (due to its dependence not only on temperature but also on multiple (non-equilibrium!) particle fugacities).

III. SPECTRA AND FLOW FROM HYDRODYNAMICS AND THE HYBRID MODEL

A. EOS dependence: s95p-PCE vs. SM-EOS Q

In this subsection we calculate transverse momentum spectra and elliptic flow for identified hadrons in the hybrid approach and compare them to pure ideal and viscous hydrodynamic calculations, focusing in particular on the EOS and the T_{dec} dependences of the calculations. The main idea of this comparison is to determine whether the results of the hybrid model calculation can be reproduced by pure ideal or viscous hydrodynamics, or if specific features in the spectra and the transverse momentum or centrality dependence of v_2 lead to clear discriminators between the two approaches. Unless otherwise noted, we use initial conditions and switching and decoupling parameters as described in Sec. II. With identical initial conditions and identical transport coefficients η/s in the hydrodynamic QGP stage, we ensure that the only difference between the **VISH2+1** and **VISHNU** runs lies in the treatment of the hadronic stage. In the SM-EOS Q(CE) case this means that the pure hydrodynamic runs assume both thermal and chemical equilibrium in the hadronic phase, whereas the **UrQMD** component of **VISHNU** breaks both. When we use **VISH2+1** with s95p-PCE, we ensure that the pure hydrodynamic and **VISHNU** hybrid simulations use the same non-equilibrium chemical composition in the hadronic stage; in this case the difference lies only in the assumption of (approximate) thermal equilibrium for the hydrodynamic runs whereas the **UrQMD** cascade in **VISHNU** allows the system to evolve far out of local thermal equilibrium, all the way to final decoupling.

The pion and proton transverse momentum spectra shown in the left panels of Fig. 1 demonstrate good agreement between the pure hydrodynamic and hybrid **VISHNU** runs as long as EOS s95p-PCE is used, i.e. as long as we ensure that the hydrodynamic simulations correctly implement the non-equilibrium chemical evolution in the hadronic phase. With the correct PCE equation of state, the hydrodynamic pion spectra are almost insensitive to the choice of kinetic decoupling temperature T_{dec} , agreeing well with their counterparts from the hybrid model **VISHNU** in all cases. The hydrodynamic proton spectra become flatter as T_{dec} decreases, due to build-up of additional radial flow, and the best agreement with the hybrid model is achieved for the lowest value shown in the graph ($T_{\text{dec}} = 100$ MeV). This demonstrates that significant additional radial flow is generated during the hadronic rescattering stage [21, 47], but that for pions (whose momentum distributions react less strongly to radial flow than the heavier protons) the radial flow and cooling effects on the spectral slope balance each other as we lower T_{dec} [35]. Figure 1 shows that all of the above statements hold irrespective of whether we assume zero or non-zero viscosity during the QGP stage: in both cases the transverse momentum spectra from the hybrid code **VISHNU** can be well represented by purely hydrodynamic simulations with $T_{\text{dec}} = 100$ MeV and η/s values that do not change between the QGP and hadron gas stages.

The right panels in Fig. 1 show that the same is not true when we use SM-EOS Q in the hydrodynamic code which assumes chemical equilibrium in the hadronic stage, contrary to the underlying microscopic **UrQMD** dynamics. In this case agreement between the pion spectra from **VISHNU** and the purely hydrodynamic simulations requires immediate decoupling at $T_{\text{sw}} = 160$ MeV, but the corresponding purely hydrodynamic proton spectra are too steep because they lack the boost from the additional radial flow developed by **UrQMD** during the hadronic stage. Lowering T_{dec} in the pure hydrodynamic runs helps with the shape of the proton spectra, but quickly eats into the total proton yield (i.e. the normalization of the proton spectra), due to annihilation with antiprotons, and simultaneously the pion spectra become too flat when compared with **VISHNU**.

We conclude that, at the level of single-particle pt spectra, it is possible to simulate the full microscopic dynamics of the **UrQMD** hadron cascade by viscous (or even ideal) fluid dynamics as long as a PCE EOS is used that correctly describes the non-equilibrium chemical composition in **UrQMD**, and one allows for the buildup of additional hadronic radial flow by setting a low decoupling temperature $T_{\text{dec}} \simeq 100$ MeV. With SM-EOS Q(CE), purely hydrodynamic simulations are unable to reproduce the **VISHNU** spectra for any choice of T_{dec} ; for the convenience of the following academic comparison of elliptic flow v_2 within these two approaches, we choose for SM-EOS Q the "historical standard value" $T_{\text{dec}} = 130$ MeV [48].

Research over the past few years has established that

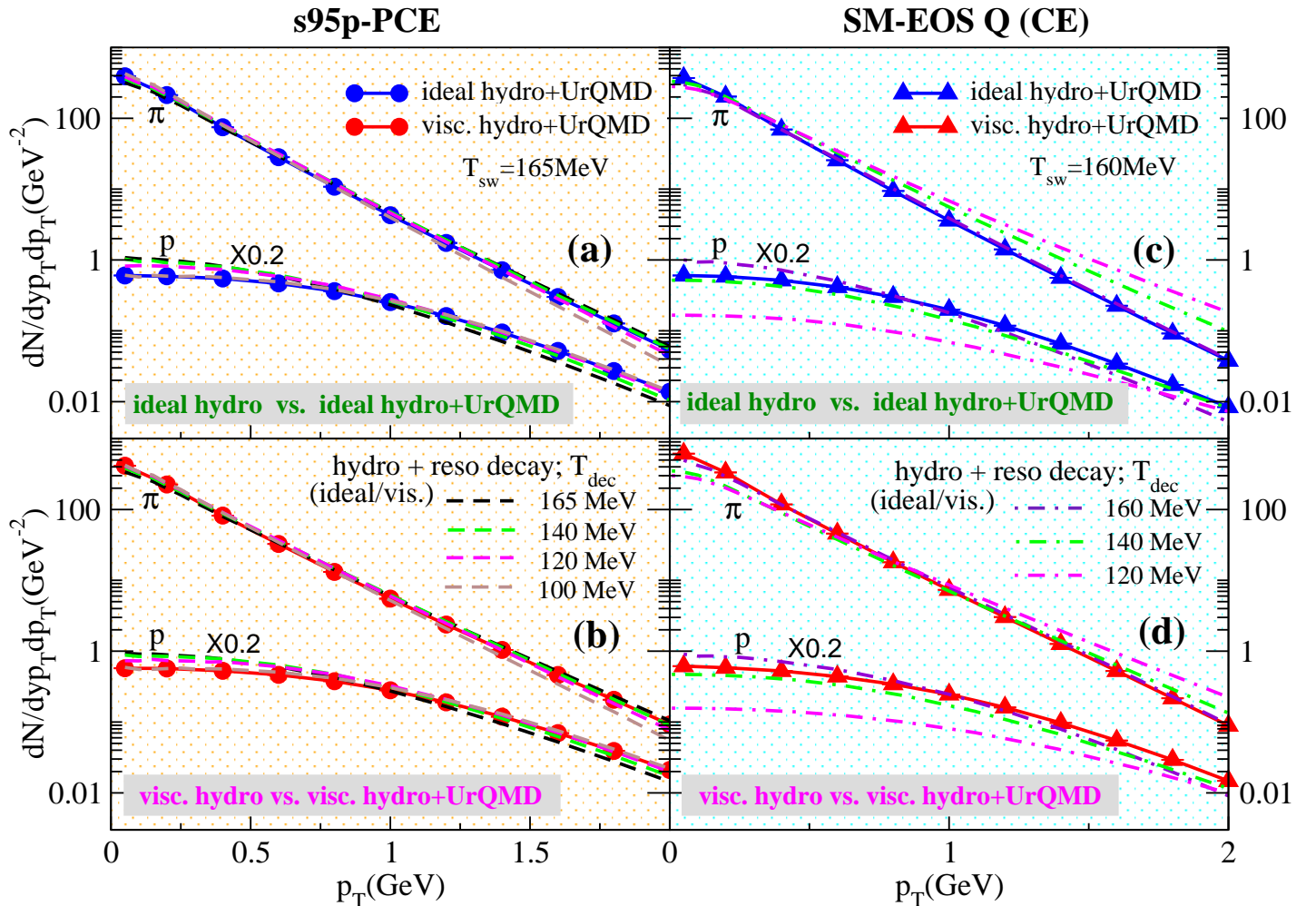


FIG. 1. (Color online) Pion and proton p_T -spectra for $b=7$ fm Au+Au, calculated from VISH2+1 and VISHNU with s95p-PCE (left panels) and SM-EOS Q(CE) (right panels). Upper panels compare pure ideal fluid dynamics and VISHNU with ideal fluid input; lower panels compare pure viscous hydrodynamics and VISHNU with viscous hydrodynamic input, using $\eta/s = 0.08$ in both cases during the fluid dynamic stage. Identical Glauber model initial conditions are used in all runs ($e_0 = 30$ GeV/fm³ at $\tau_0 = 0.6$ fm/c).

elliptic flow v_2 is influenced by both hadronic dissipative effects [22] and the chemical composition of the hadronic matter [34]. The reaction dynamics modeled by UrQMD contains both types of non-equilibrium effects. To isolate the effect of kinetic non-equilibrium we can compare results from VISHNU with pure hydrodynamic calculations that model the same hadronic chemical non-equilibrium composition as UrQMD, by using EOS s95p-PCE. This is shown in Fig. 2(a), for both an ideal ($\eta/s = 0$) and minimally viscous $\eta/s = 0.08$ QGP fluid. For $(\eta/s)_{\text{QGP}} = 0$ one finds that in the hybrid model calculations v_2 is suppressed by $\sim 15\%$ at $p_T = 2$ GeV, as a result of the hadronic viscosity inherent in the UrQMD dynamics. For $\eta/s = 0.08$ the difference between the purely hydrodynamic and hybrid model results is a bit less ($\sim 10\%$) since now the non-zero hydrodynamic viscosity already partially accounts for the viscous v_2 suppression in UrQMD. Comparing the ideal and viscous pure hydrodynamic results with each other we find $\sim 20\%$ viscous v_2 suppression at $p_T = 2$ GeV for $\eta/s = 0.08$, consistent with earlier results [8–10]. Fig. 2(a) demonstrates that evolution with the hybrid model suppresses v_2 more strongly than viscous hydrodynamics alone with the same η/s ; a realistic

microscopic description of dissipative hadron dynamics within a hybrid approach is therefore essential.⁹

Figure 2(b) shows that an incomplete separation of chemical and kinetic non-equilibrium effects can lead to misleading conclusions. Using a chemical equilibrium EOS (SM-EOS Q) in the hadronic phase and comparing a pure ideal fluid calculation with a VISHNU simulation with ideal fluid input (which is out of chemical equilibrium during most of the hadronic stage) happens to yield (at least for $b=7$ fm in Au+Au¹⁰) almost identical results for $v_2(p_T)$. Viscous suppression of v_2 by kinetic non-equilibrium [22] almost exactly balances [21]

⁹ We will see below that merely adjusting the specific shear viscosity η/s to larger values in the hadronic phase is not sufficient.

¹⁰ When compared with experiment, the hybrid model calculations exhibit a significantly improved centrality dependence compared to pure ideal fluid dynamics. The almost perfect cancellation of kinetic and chemical non-equilibrium effects on $v_2(p_T)$ seen in Fig. 2(a) may therefore not work as well at other impact parameters, although the tendency of the two effects to work against each other is generic [25].

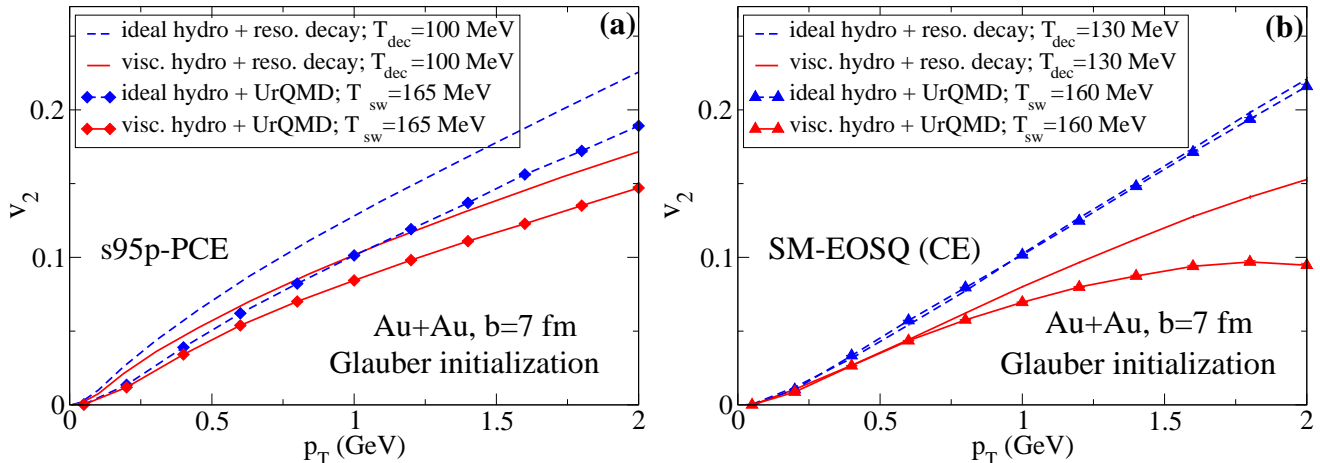


FIG. 2. (Color online) $v_2(p_T)$ for all hadrons from $b=7$ fm Au+Au collisions, calculated from VISH2+1 (lines without symbols) and VISHNU (lines with symbols). Dashed and solid lines are for ideal ($\eta/s=0$) and viscous ($\eta/s=0.08$) fluids during the hydrodynamic stage, with EOS s95p-PCE (a) and SM-EOSQ Q(CE) (b), respectively. Same initial conditions as in Fig. 1.

the previously observed enhancement of $v_2(p_T)$ caused by chemical non-equilibrium in the hadronic phase [32–34]. The solid lines comparing pure viscous hydrodynamics and VISHNU with viscous fluid input demonstrate that this cancellation is accidental and no longer occurs when describing the QGP as a viscous fluid. In this case VISHNU gives much lower $v_2(p_T)$ than the pure viscous hydrodynamic calculation, mainly caused by large negative contributions from the viscous correction δf to the local distribution function on the switching surface which the subsequent UrQMD dynamics is unable to erase. Viscous hydrodynamics with constant η/s in the hadronic phase, on the other hand, evolves back towards local thermal equilibrium such that on the final decoupling surface at T_{dec} only small δf contributions remain.¹¹

B. Hadronic contribution to elliptic flow

Having established that identical chemical compositions in the pure hydrodynamic and hybrid model evolutions are essential for a meaningful comparison that aims to assess dissipative effects in the hadronic stage, we will from now on use the chemically frozen EOS s95p-PCE in all simulations.

In Fig. 3 we compare the differential pion and proton elliptic flow, $v_2(p_T)$, from VISHNU (solid lines with symbols) with pure fluid dynamical calculations, implementing kinetic freeze-out either directly at $T_{\text{sw}} = T_{\text{chem}} = 165$ MeV (dashed lines with symbols) or at $T_{\text{dec}} = 100$ MeV (solid lines without symbols). The curves in panel (a) and (b) assume $\eta/s=0$ and $\eta/s=0.08$, respectively, during the fluid dynamic stage. We focus our

attention on the mass splitting between pions and protons. The smallest mass splitting is found for immediate decoupling at T_{sw} (dashed lines). Hadronic rescattering in VISHNU (solid lines with symbols) increases the mass splitting at low p_T , by pushing $v_2(p_T)$ up for pions and towards larger p_T for protons [47]. Both of these effects strengthen if we replace the microscopic hadronic rescattering cascade by macroscopic hydrodynamic evolution [47]. The depletion of proton v_2 at small p_T is a consequence of additional radial flow buildup in the hadronic stage which pushes the heavy protons more efficiently than the light pions to larger transverse momenta (see Fig. 1); the larger $v_2(p_T)$ for low- p_T pions reflects (at least partially) a simultaneous increase of the total momentum anisotropy, in response to the remaining spatial fireball eccentricity that survives into the hadronic stage. These effects are qualitatively similar for ideal (Fig. 3a) and viscous fluids (Fig. 3b), although the larger δf corrections at T_{sw} in viscous hydrodynamics lead to an additional downward shift of $v_2(p_T)$ for both pions and protons at large p_T when hadronic rescattering is turned off (dashed lines).

C. Viscous v_2 suppression

Figure 4 shows the net effect of the hadronic medium modifications of the transverse momentum spectra and differential elliptic flow on the p_T -integrated charged hadron v_2 , as a function of collision centrality (parametrized by the number of participants N_{part}). The smallest amount of v_2 is obtained without any hadronic rescattering at all (dashed lines), with an additional suppression of about 20% for the minimally viscous fluid ($\eta/s=0.08$) relative to the ideal fluid. The UrQMD module in the hybrid code VISHNU creates about 15% additional v_2 via hadronic rescattering, but a hydrodynamic

¹¹ This is, of course, an academic comparison since viscous hydrodynamics with constant η/s cannot consistently account for hadronic freeze-out.

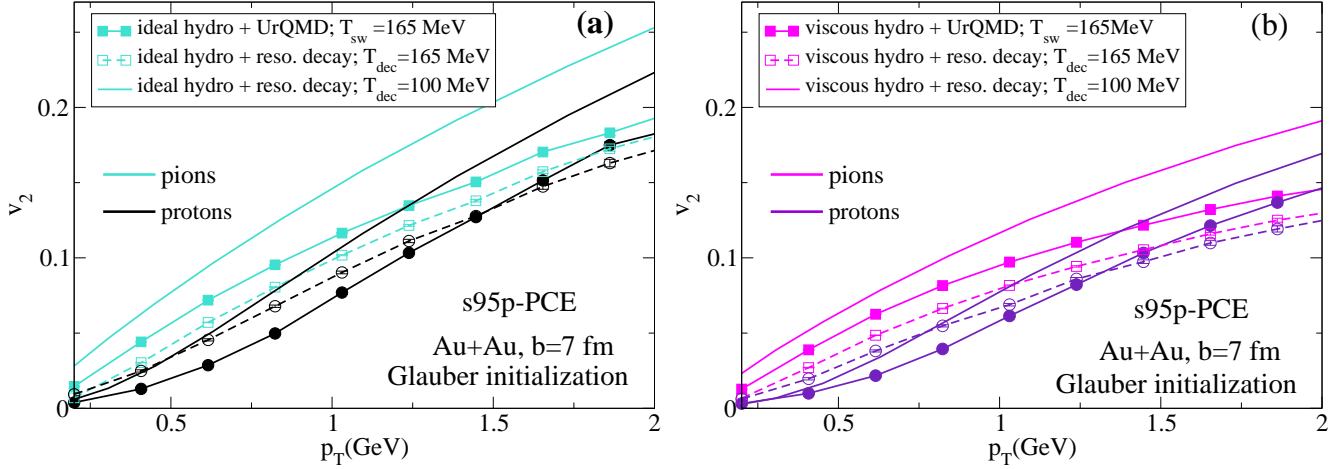


FIG. 3. (Color online) Differential elliptic flow $v_2(p_T)$ for pions (light blue/magenta) and protons (black/purple) from $b=7$ fm Au+Au collisions. Results from the hybrid model VISHNU (solid lines with solid symbols) are compared with purely hydrodynamic simulations for $\eta/s=0$ (a) and $\eta/s=0.08$ (b) for decoupling temperatures $T_{\text{dec}}=165$ MeV (dashed with open symbols) and $T_{\text{dec}}=100$ MeV (solid without symbols). All calculations use EOS s95p-PCE in the hydrodynamic stage. Initial conditions are the same as in Fig. 1. Please note the suppressed zeroes on the horizontal axes.

description of the hadron gas, treating it either as an ideal or a minimally viscous fluid, generates a much larger hadronic contribution to v_2 . This reflects the fact that in the hadronic stage the fireball is still out-of-plane elongated, and demonstrates that even a viscous fluid with $\eta/s=0.08$, but especially an ideal fluid is much more efficient than UrQMD in converting this residual fireball eccentricity into additional elliptic flow.

To quantify the suppression of integrated elliptic flow by viscous QGP and hadronic dissipation effects we define the ratio

$$v_2^{\text{supp.}} = \frac{v_2^{\text{A}} - v_2^{\text{B}}}{v_2^{\text{A}}}$$

where A and B denote two different dynamical evolu-

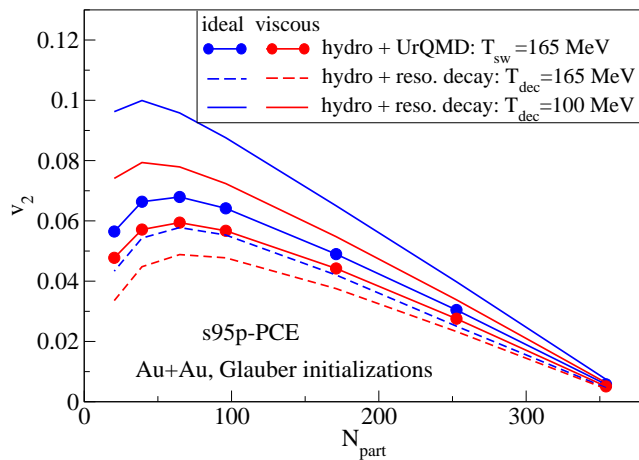


FIG. 4. (Color online) Centrality dependence of the p_T -integrated elliptic flow of all hadrons, for the same parameters as in Fig. 3.

tion models. Figure 5a shows that viscous suppression effects are generically larger in peripheral than in central collisions, due to the smaller fireball sizes. The solid line in panel (a) confirms the naive expectation that the strongest suppression (here 30–50%, depending on collision centrality) should be seen when comparing VISHNU with viscous fluid input to a purely hydrodynamic, ideal fluid simulation. Among the combinations studied in Fig. 4, this case maximizes the suppression of elliptic flow by combining (in the VISHNU simulation) viscous effects in the QGP with large dissipative effects in the hadronic stage. Replacing the UrQMD part of the evolution by viscous hydrodynamics with $\eta/s=0.08$ (dashed line) yields only about half of the viscous v_2 suppression observed in VISHNU. The smallest suppression ratio ($\sim 10-15\%$) is found between VISHNU simulations with ideal and viscous fluid input at T_{sw} (dot-dashed line in Fig. 5a).

These observations indicate that, in Au+Au collisions at RHIC with $(\eta/s)_{\text{QGP}} = \mathcal{O}(\frac{1}{4\pi})$, hadronic dissipative effects play a larger role for the finally observed v_2 than QGP viscosity. This conclusion is reinforced by Fig. 5b which shows (depending on centrality) 20–40% v_2 suppression just from hadronic dissipation. The VISH2+1 and VISHNU comparison runs for $\eta/s=1/(4\pi)$ show relatively less suppression of v_2 by hadronic dissipation in UrQMD since the non-zero η/s already suppresses hadronic v_2 generation in the purely hydrodynamic run.

Obviously, the hadronic rescattering stage described by UrQMD is much more dissipative than both an ideal ($\eta/s=0$) and a “perfect” (i.e. minimally viscous, $\frac{\eta}{s} = \frac{1}{4\pi}$) fluid. This raises the question whether we could perhaps simulate the hadronic rescattering cascade hydrodynamically by making the fluid more viscous on the hadronic side of the quark-hadron phase transition. The answer to this question is explored in the following section.

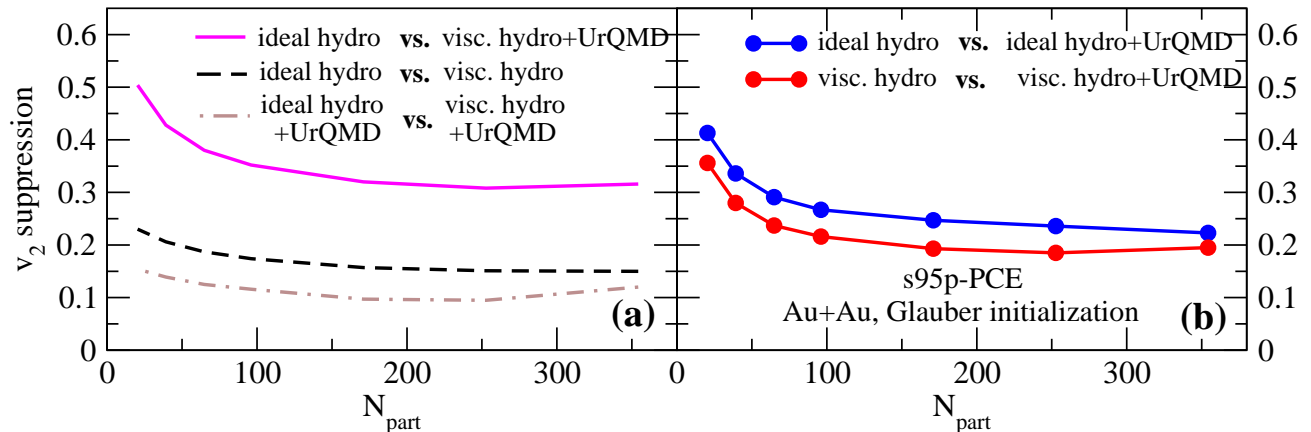


FIG. 5. (Color online) Viscous v_2 suppression between different lines shown in Fig. 4.

IV. VISHNU WITH LOWER SWITCHING TEMPERATURES AND A TEMPERATURE DEPENDENT HADRONIC $(\eta/s)(T)$

Hydro+cascade hybrid approaches that use in their hydrodynamic modules an equation of state that assumes chemical equilibrium in the hadron resonance gas have little choice where to switch from the macroscopic fluid dynamic to the microscopic Boltzmann picture: If they want to correctly reproduce the experimentally measured final hadron yields which reflect chemical freeze-out at $T_{\text{chem}} \simeq 165$ MeV, the switching must be done at that temperature. With the chemically frozen EOS s95p-PCE we can also select lower switching temperatures and, in doing so, explore the existence of a “switching window” within which, using appropriately adjusted transport coefficients for the hydrodynamic evolution, both macroscopic and microscopic descriptions can be used interchangeably, without affecting the final outcome.

To judge the validity of using hydrodynamics to emulate microscopic UrQMD dynamics we check the final pion and proton transverse momentum spectra and their differential elliptic flow $v_2(p_T)$. We do so for a fixed impact parameter $b=7$ fm which for the Au+Au collision system is known to also provide a fair representation of the spectra and elliptic flow from minimum bias collisions.

The most sensitive and robust [12] observable that will dictate our (temperature dependent) choice of η/s in the hadronic phase is the integrated elliptic flow v_2 . Strictly speaking, it is controlled by both the shear viscosity and the associated microscopic relaxation time τ_π that controls the speed with which the shear pressure tensor $\pi^{\mu\nu}$ approaches its Navier-Stokes limit [10]. In kinetic transport theory, both η and τ_π involve integrals over the same collision kernel and are typically proportional to each other [49]. In the QGP, where η/s is small, τ_π is therefore short of order 0.2 fm, leading to rapid memory loss and insensitivity of the developing elliptic flow to initial conditions for the viscous pressure [10]. If, however, η/s becomes large in the hadronic phase [45, 50–52], one

should expect the corresponding relaxation time to grow similarly, with a constant of proportionality between the dimensionless combinations η/s and $T\tau_\pi$ that may be different and possibly larger in the hadronic than in the QGP phase.

Unfortunately, with our present code setup an independent determination of the temperature dependence of η/s and $T\tau_\pi$ in the hadronic stage (from a comparison of VISHNU simulations with different T_{sw} values) is too time consuming and thus not practical. We have therefore focused our attention on the extraction of $(\eta/s)(T)$, holding the relation $T\tau_\pi = 3\eta/s$ fixed at all temperatures.

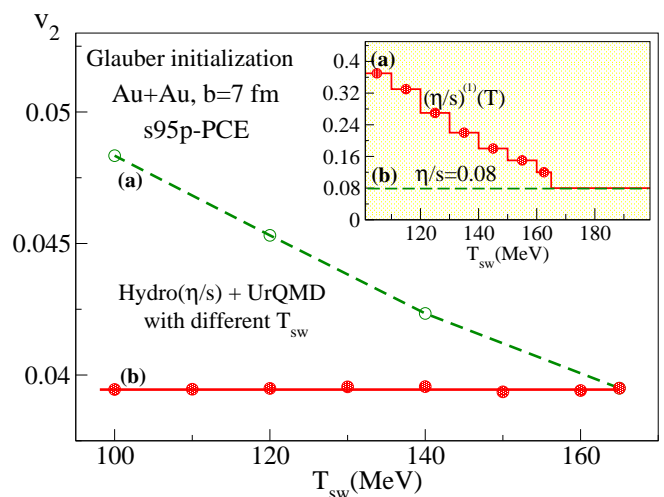


FIG. 6. (Color online) Integrated v_2 for pions for $b=7$ fm Au+Au, calculated from VISHNU with different switching temperatures T_{sw} . Case (a) assumes constant $\eta/s=0.08$ in VISH2+1, whereas case (b) uses the temperature dependent $(\eta/s)^{(1)}(T)$ shown in the inset, which was extracted from the integrated pion v_2 as described in the text.

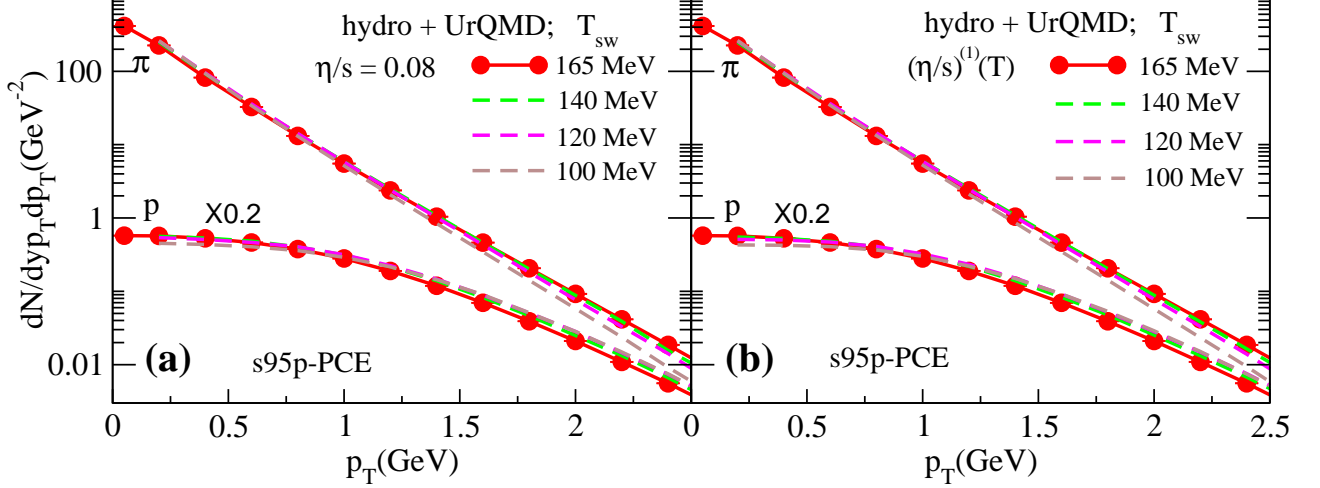


FIG. 7. (Color online) Pion and proton p_T -spectra from $b=7$ fm Au+Au collisions, calculated with VISHNU using different switching temperatures T_{sw} and constant ($\eta/s=0.08$, panel (a)) or temperature dependent ($(\eta/s)^{(1)}(T)$ from Fig. 6, panel (b)) shear viscosities in the hydrodynamic stage.

A. Effective $(\eta/s)(T)$ from UrQMD with VISH2+1 input

The green dashed line in Fig. 6 shows that, if we couple VISH2+1 with constant specific entropy $\eta/s=0.08$ to UrQMD at lower and lower switching temperatures, we obtain larger and larger values for the total pion v_2 . Obviously, the hydrodynamic evolution between $T_{chem}=165$ MeV and $T_{sw} < T_{chem}$ generates more additional elliptic flow than propagation of the hadrons with UrQMD during the same temperature interval. This suggests that UrQMD in the temperature region $T_{sw} < T < T_{chem}$ has a larger effective shear viscosity η/s than 0.08. By lowering the switching temperature from the starting value $T_{sw}=165$ MeV in small steps ΔT and adjusting, step by step, η/s in the interval $[165 \text{ MeV} - n\Delta T, 165 \text{ MeV} - (n-1)\Delta T]$ such that no additional pion v_2 is generated when we replace UrQMD evolution in this temperature interval by VISH2+1 with this adjusted η/s value, we arrive at the effective temperature dependent $(\eta/s)^{(1)}(T)$ shown in the inset of Fig. 6) that ensures a constant pion elliptic flow v_2 that is independent of the switching temperature (flat horizontal line in Fig. 6). Note that this is a time consuming and labor-intensive iterative procedure that cannot be short-circuited since the effective η/s extracted for the n^{th} interval turns out to depend on the previously determined effective $(\eta/s)^{(1)}(T)$ values for smaller n values, i.e. at higher temperatures.

B. Testing the effective $(\eta/s)^{(1)}(T)$ from UrQMD

Starting at the QGP input value of $\eta/s=0.08$, the thus extracted effective $(\eta/s)^{(1)}(T)$ increases by almost a factor 5 between $T=T_{chem}=165$ MeV and $T=100$ MeV, growing roughly linearly with decreasing temperature.

Figure 7 shows that this has very little effect on the pion and proton p_T -distributions: Whether one uses constant $\eta/s=0.08$ (panel (a)) or the temperature dependent $(\eta/s)^{(1)}(T)$ from Fig. 6 (panel (b)), the transverse momentum spectra for both pions and protons exhibit very little dependence on the switching temperature T_{sw} . Just as for the pure hydrodynamic calculations shown in Fig. 1, lower switching temperatures lead to slightly flatter spectra for protons (where the hadronic buildup of additional radial flow overwhelms the cooling effect) and to slightly steeper spectra for pions (for which the cooling effect dominates). Very little of the difference in the final spectra that can be attributed to the different hadronic viscosities used in the two panels of Fig. 4.

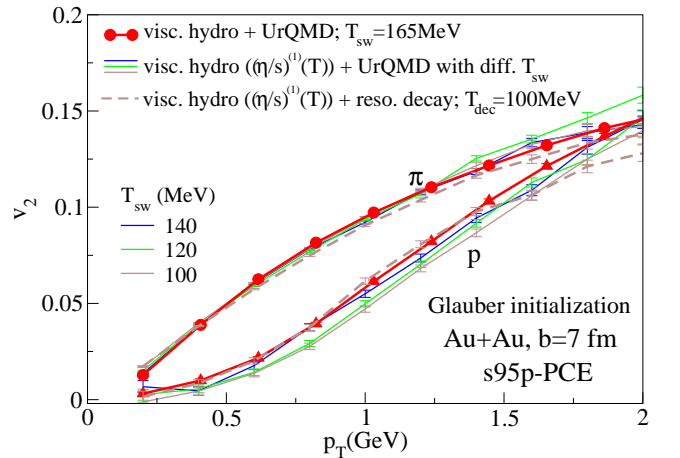


FIG. 8. (Color online) Differential $v_2(p_T)$ for pions and protons in $b=7$ fm Au+Au collisions, calculated by matching viscous hydrodynamics with temperature dependent $(\eta/s)^{(1)}(T)$ (see Fig. 6) to UrQMD at different switching temperatures T_{sw} .

For the elliptic flow the temperature dependence mat-

ters, as Figure 6 clearly demonstrates. However, Figure 8 shows that, when using the “correct” temperature dependent $(\eta/s)^{(1)}(T)$ in the VISH2+1 module, VISHNU produces not only T_{sw} -independent *integrated* pion elliptic flow (by construction), but also approximately T_{sw} -independent p_T -*differential* elliptic flow $v_2(p_T)$ for both pions and protons. Still, when looking at the details one observes a difference between the solid and dashed brown lines for protons which shows that decoupling VISH2+1 at $T_{\text{dec}} = 100$ MeV into non-interacting particles is *not* the same as switching from VISH2+1 to UrQMD at $T_{\text{sw}} = 100$ MeV and letting UrQMD do the kinetic freeze-out: there obviously is some rescattering of protons in UrQMD occurring at temperatures below 100 MeV, caused by “pion wind” [53], that moves the protons to larger p_T and depletes the proton elliptic flow at low p_T . Since the solid brown line, corresponding to hydrodynamic evolution down to 100 MeV followed by UrQMD freeze-out, is different from the solid red line with triangles, which corresponds to a switch from hydrodynamics to UrQMD already at 165 MeV, we see that even with the “correct” temperature dependent $(\eta/s)^{(1)}(T)$ hydrodynamic evolution with VISH2+1 differs somewhat from UrQMD. However, the difference is small, and for pions its consequences are almost negligible.

Figures 9 and 10 show that the same $(\eta/s)^{(1)}(T)$ extracted in Fig. 6 from simulations with optical Glauber model initial conditions also works for CGC motivated initial conditions that are obtained by averaging over many fluctuating initial entropy density profiles (see Sec. II A) and thus account for the large effects from event-by-event fluctuations on the average initial source eccentricity in very central and very peripheral events. For all three centrality classes shown in these two figures we see that using the temperature dependent $(\eta/s)^{(1)}(T)$ extracted from Fig. 6 for the hydrodynamic evolution yields values for the integrated pion elliptic flow v_2 (Fig. 9) and shapes for the p_T -differential pion elliptic flow $v_2(p_T)$ (Fig. 10) that are independent of the switching temperature T_{sw} down to $T_{\text{sw}} = 120$ MeV (we did not probe any lower). This is not trivial since the initial source eccentricities (and thus the produced elliptic flows) for the centralities shown here are 20–50% larger than the optical Glauber ones.

In the most peripheral bin (60-70%) things begin to break down around $T_{\text{sw}} = 120$ MeV. The increase of integrated v_2 and of $v_2(p_T)$ at low p_T seen in Figs. 9 and 10 for $T_{\text{sw}} = 120$ MeV indicates stronger dissipative effects in UrQMD at low T than captured by effective $(\eta/s)^{(1)}(T)$ from Fig. 6. In peripheral collisions (i.e. for small fireballs) VISH2+1 apparently can no longer accurately mimic the microscopic kinetic evolution of UrQMD at low temperatures $T_{\text{sw}} \sim 120$ MeV and should therefore not be used under such conditions.

We can summarize the findings of this subsection in the following statement: By using the temperature-dependent $(\eta/s)^{(1)}(T)$ extracted in Sec. IV A from the integrated pion elliptic flow by comparing microscopic

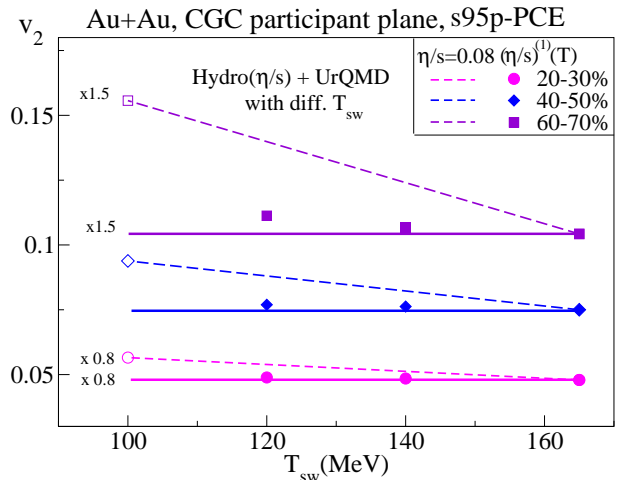


FIG. 9. (Color online) Pion v_2 for Au+Au collisions of different centralities (bottom set: 20-30%; middle set: 40-50%; top set: 60-70%), calculated with VISHNU using constant $\eta/s = 0.08$ (dashed lines) or temperature dependent $(\eta/s)^{(1)}(T)$ (solid lines) in the fluid dynamic stage. In contrast to Figs. 6 and 7, we here use averaged fluctuating fKLN initial conditions.

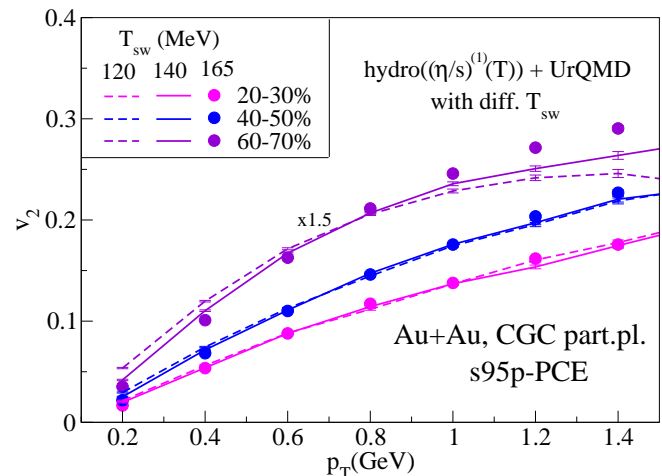


FIG. 10. (Color online) Differential $v_2(p_T)$ for pions. Same parameters and color coding as in Fig. 9.

and macroscopic simulations of the hadron gas phase below T_{chem} , the macroscopic evolution code VISH2+1 provides a fair description of the microscopic UrQMD dynamics down to temperatures around 120 MeV. When used in hybrid mode together with UrQMD (as implemented in VISHNU), it yields transverse momentum distributions of pions and protons (including their elliptic flow $v_2(p_T)$) that are, to good approximation, independent of the switching temperature in the window $120 \text{ MeV} \leq T_{\text{sw}} \leq 165 \text{ MeV}$. This raises, however, two questions:

- Is $(\eta/s)^{(1)}(T)$ a genuine medium property of the hadronic matter described by UrQMD? If it is, it

should be independent of the viscous hydrodynamic input into UrQMD. So far we have only shown results where the UrQMD input was obtained from hydrodynamic simulations of the earlier QGP evolution with a single viscosity value $(\eta/s)_{\text{QGP}} = 0.08$. If the QGP has a larger or smaller viscosity, will UrQMD continue to propagate the correspondingly modified hydrodynamic input at T_{sw} as if it were a viscous fluid with temperature dependent $(\eta/s)^{(1)}(T)$?

- The $(\eta/s)^{(1)}(T)$ values shown in the inset of Fig. 6 are much smaller (especially in the region just below $T_{\text{chem}} \approx T_c$) than those computed in Ref. [45] using the Kubo formula. The Kubo formula evaluates a thermal equilibrium ensemble expectation value of a spectral density operator, whereas the procedure of Sec. IV A extracts the transport coefficient from a comparison of the dynamical output produced by two different evolution models in a rapidly expanding medium. What is the reason for these different shear viscosities?

In the following subsection we describe a study that yields at least partial answers to these questions.

C. Non-universality of the effective UrQMD viscosity $(\eta/s)^{(1)}(T)$

To address the first question we redid the analysis of Sec. IV A using a twice larger QGP viscosity, $(\eta/s)_{\text{QGP}} = 0.16$. This means that the UrQMD module of VISHNU is initialized with somewhat different density and flow profiles and, in particular, a shear viscous pressure tensor $\pi^{\mu\nu} \approx 2\eta\sigma^{\mu\nu}$ that is roughly twice as large as before when we used $(\eta/s)_{\text{QGP}} = 0.08$.¹² Going through the same iterative procedure as before of adjusting the specific shear viscosity η/s temperature interval by temperature interval such that it generates in VISH2+1 exactly the same amount of total pion v_2 as UrQMD, we obtain the upper set of solid green dots in Fig. 11, labeled as $(\eta/s)^{(2)}(T)$. It is obviously different from and larger than $(\eta/s)^{(1)}(T)$. In particular, at the highest switching temperature $T_{\text{sw}} = 165$ MeV, $(\eta/s)^{(2)}(T)$ starts out close to the value of 0.16 used in the evolution of the QGP stage, whereas $(\eta/s)^{(1)}(T)$ starts out almost half as small, with a magnitude close to the QGP value of 0.08 used in the first extraction.

The “effective UrQMD viscosity” $(\eta/s)(T)$ extracted by this procedure apparently “remembers” the prior QGP history of the fireball and its transport properties. This

means that it does not describe an intrinsic medium property of the hadron resonance gas in UrQMD. Further insight into this puzzle is gained by looking at the purple dashed line and open squares in Fig. 11, labeled by $(\eta/s)^{(3)}(T)$: Here we initialize UrQMD with viscous hydrodynamic output from a run with $(\eta/s)_{\text{QGP}} = 0.16$, but assume that just before hadronization, at a temperature of 180 MeV, the QGP viscosity suddenly drops to half that value, $(\eta/s)_{\text{QGP}} = 0.08$. In this case, the extracted “effective UrQMD viscosity” $(\eta/s)^{(3)}(T)$ comes out identical to $(\eta/s)^{(1)}(T)$, i.e. as if the QGP phase had evolved with minimal shear viscosity throughout its life, and not just at the very end of its history after its temperature dropped below 180 MeV.

Evolving the QGP medium from identical initial conditions with a twice larger η/s value of 0.16 leads to noticeably different density and flow profiles on the $T_{\text{sw}} = 165$ MeV switching surface compared to those for $\eta/s = 0.08$. These differences cannot be undone by changing η/s back to 0.08 within 15 MeV of the critical temperature. The equality of $(\eta/s)^{(1)}(T)$ and $(\eta/s)^{(3)}(T)$ shows that they are not controlled by the energy density and flow velocity profiles on the switching surface (which are different for the solid red and dashed purple lines), but instead by the shear pressure tensor. Due to the short relaxation times τ_π in the QGP phase, we can approximate $\pi^{\mu\nu} \approx 2\eta\sigma^{\mu\nu}$, so a factor of 2 difference in η/s leads to roughly a factor 2 difference in $\pi^{\mu\nu}$ on the switching surface. (The differences in the entropy density and velocity shear tensor, although noticeable, are not anywhere close to a factor 2.) At this level of precision, the hydrodynamic output corresponding to the green solid line (from a QGP evolving with $(\eta/s)_{\text{QGP}} = 0.16$ all the way to $T_{\text{sw}} = 165$ MeV) features a viscous pressure $\pi^{\mu\nu}$ that is twice as big as that for the red solid line ($(\eta/s)_{\text{QGP}} = 0.08$), whereas the one corresponding to the

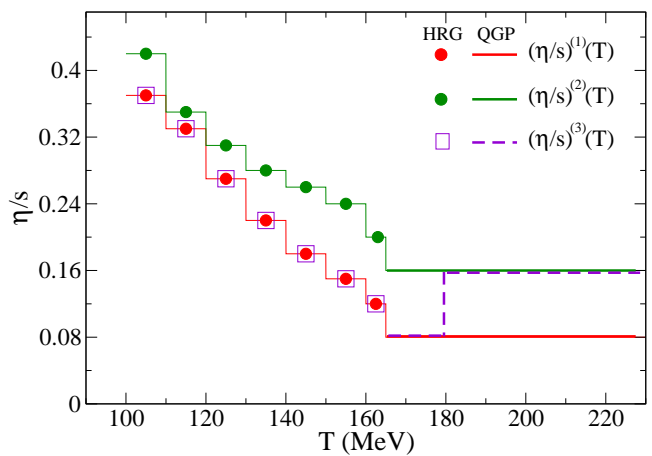


FIG. 11. (Color online) Temperature dependent effective $(\eta/s)(T)$ extracted as in Fig. 6 from viscous hydrodynamic emulations of UrQMD dynamics, for three different viscous fluid initializations of the UrQMD stage (see text for discussion).

¹² Here $\sigma^{\mu\nu} = \nabla^{(\mu} u^{\nu)}$ is the velocity shear tensor, see [10] for details. Since η/s is small in the QGP, the associated relaxation time τ_π is much shorter than the inverse of the local expansion rate on the switching surface, hence $\pi^{\mu\nu}$ does not stray far from its Navier-Stokes value $\pi^{\mu\nu} = 2\eta\sigma^{\mu\nu}$ on that surface.

purple dashed line is roughly equal to that of the red solid line. The “effective UrQMD viscosities” $(\eta/s)^{(n)}(T)$ seem to reflect and remember these relationships.

We can understand this by recalling the kinetic theory relation $\pi^{\mu\nu} = \int \frac{d^3p}{E} p^{(\mu} p^{\nu)} \delta f$ between the viscous pressure tensor and the deviation δf of the phase-space distribution function from local thermal equilibrium. The value of $\pi^{\mu\nu}$ on the switching surface controls the magnitude of the non-equilibrium contribution $\delta f \sim p^\mu p^\nu \pi_{\mu\nu}$ to the hadron momentum distributions sampled by the hydro-to-micro converter H₂O which generates the UrQMD input. Apparently, collisions and other interactions in UrQMD are too infrequent or inefficient in transferring momenta to quickly relax these non-equilibrium distributions. As long as the deviations δf persist in a form close to their initial values, they contribute a term $\pi^{\mu\nu}$ to the UrQMD energy-momentum tensor that, if one writes it in hydrodynamic language as $\pi^{\mu\nu} = 2\eta\sigma^{\mu\nu}$, requires a value of η/s that is close to the value used in the generation of the UrQMD input with H₂O. As UrQMD evolves the momentum distributions, $\pi^{\mu\nu}$ evolves, too, and when we fit the VISH2+1 transport properties to those of the UrQMD cascade assuming short relaxation times, we end up fitting this evolving $\pi^{\mu\nu}$ instead of extracting a genuine transport coefficient for UrQMD.

The $(\eta/s)^{(n)}(T)$ curves shown in Fig. 11 exhibit a tendency to approach each other at lower temperatures. This may suggest a loss of memory of the initial viscous pressure components on a time scale comparable to the cooling time needed to cool the system from $T_{\text{chem}} = 165$ MeV to somewhere around 100 MeV. This time is longer than the one assumed in our viscous hydrodynamic simulations of the UrQMD stage, $T\tau_\pi = 3\eta/s$. Indeed, there are other indications [54] that UrQMD may have a much longer relaxation time than given by the classical kinetic theory result for massless Boltzmann particles, $\tau_\pi = 6\eta/(sT)$ [55]. For the time being, further exploration of this issue will have to wait.

V. DISCUSSION AND CONCLUSIONS

In this article we presented VISHNU, a new hybrid approach for the bulk evolution of viscous QCD matter created in ultrarelativistic heavy-ion collisions that combines a macroscopic viscous hydrodynamic description of the early (dense) QGP phase with a microscopic Boltzmann cascade for the late (dilute) hadron resonance gas stage. The model merges the economy of a macroscopic description for the first 4–10 fm/c (depending on centrality) after thermalization, when the matter is close to local thermal equilibrium, with the precision of a microscopic approach for the late hadronic stage when, after hadronization of the QGP, the mean free paths for the hadronic medium constituents increase rapidly, the matter moves farther and farther away from local equilibrium, and finally decouples into non-interacting, free-streaming particles.

The hydrodynamic and Boltzmann cascade components of VISHNU are connected via the hydro-to-micro converter H₂O, a Monte Carlo event generator that samples the Cooper-Frye phase-space distributions from the viscous hydrodynamic output along a switching surface of constant temperature T_{sw} and injects the resulting particles into UrQMD for further microscopic propagation.

By using a microscopic cascade approach for the late hadronic stage in heavy-ion collisions, the complex microscopic dynamics of chemical and kinetic freeze-out is accounted for without extraneous parameters, removing a major source of uncertainty in connecting final hadron spectra with transport properties of the initial QGP phase. With the help of VISHNU a reliable extraction of the QGP shear viscosity $(\eta/s)_{\text{QGP}}$ from experimental RHIC data, with good theoretical control of the associated uncertainties, has now become possible [12].

In default mode, VISHNU is used with switching temperature $T_{\text{sw}} = T_{\text{chem}} = 165$ MeV. Since the experimentally determined chemical freeze-out temperature $T_{\text{chem}} \approx 165$ MeV [28] approximately agrees with the best presently available theoretical estimate for the (pseudo)critical temperature for the chiral phase transition in QCD [26, 27], this is the highest temperature for which a microscopic description in terms of colliding hadrons with vacuum masses and decay widths makes sense, i.e. the highest temperature for which UrQMD can be reliably used. In default mode the system is therefore described by a chemical equilibrium EOS in the hydrodynamic stage, followed by a microscopic stage in which first chemical and then kinetic equilibrium are broken automatically by the microscopic scattering dynamics. In this mode no chemically frozen EOS is needed.

The main thrust of the present work has been to investigate whether VISHNU can be used with lower switching temperatures. Since the microscopic evolution of the hadron resonance gas via UrQMD is numerically much more costly than a macroscopic hydrodynamic description, one would like to use hydrodynamics as long as possible and switch to UrQMD only when the macroscopic approach is no longer reliable. We showed that in that case using a chemically frozen hadron resonance gas EOS in the hydrodynamic evolution below T_{chem} is compulsory. Without such a realistic EOS, which takes into account that at temperatures below T_{chem} the stable particle yields must not change anymore, one cannot find a single value for the kinetic decoupling temperature in VISH2+1 that simultaneously reproduces the microscopically evolved pion and proton transverse momentum spectra from VISHNU. For the differential elliptic flow $v_2(p_T)$ using a chemical equilibrium hadronic EOS can lead to quite misleading results.

Using the chemically frozen EOS s95p-PCE [24, 25] one finds that, with the judicious choice $T_{\text{dec}} = 100$ MeV for the kinetic decoupling temperature, the pion and proton spectra from VISHNU can be reasonably well reproduced by a purely hydrodynamic calculation with VISH2+1, without even a need for changing the specific shear vis-

cosity η/s between the QGP and HRG stages. The same does not hold, however, for the elliptic flow: since at RHIC energies the fireball is still out-of-plane elongated when its matter enters the HRG phase, the momentum anisotropy continues to grow during the hadronic stage, and **UrQMD** is less efficient in converting the residual source eccentricity into elliptic flow than **VISH2+1** if one uses the same minimal η/s in both phases. Since we also showed that, under RHIC conditions, the total suppression of elliptic flow below its ideal fluid limit is dominated by the hadronic stage (Fig. 5), this demonstrates unequivocally that, if one wants to avoid or minimize the cost of using a microscopic approach like **UrQMD**, great care must be taken to use the correct transport properties of the hadronic phase in **VISH2+1** below T_c .

We therefore tried to improve the hydrodynamic description of the HRG by increasing η/s in the hadronic phase. To extract the temperature dependence of η/s in the hadronic phase as described by **UrQMD**, we lowered T_{sw} in small intervals and adjusted η/s in **VISH2+1** in each newly covered temperature interval such that **VISH2+1** produced exactly as much additional v_2 for pions as **VISHNU** resp. **UrQMD** did. We found a function that we called $(\eta/s)^{(1)}(T)$ that started at $T_{sw} = T_{chem}$ close to the value used in the QGP phase and then increased dramatically, by almost a factor 5, as we lowered T_{sw} to 100 MeV. Surprisingly, this $(\eta/s)^{(1)}(T)$ was much smaller than the corresponding values previously extracted from **UrQMD** using the Kubo formula [45].

With this $(\eta/s)^{(1)}(T)$, **VISH2+1** is able to reproduce quite well the transverse momentum spectra as well as not only the integrated, but also the p_T -differential elliptic flow of pions and protons calculated with the full hybrid code **VISHNU** (Figs. 7 and 8). It continues to do so if we replace the optical Glauber model initial conditions in **VISH2+1** by an ensemble average of fluctuating initial conditions from the **fKLN** model (Figs. 9 and 10). But it fails badly when we replace the hydrodynamic input into **UrQMD** by one that was calculated with a different $(\eta/s)_{QGP}$. In fact, the effective hadronic $(\eta/s)(T)$ extracted from **UrQMD** by demanding that both **VISH2+1** and **VISHNU** produce the same total pion elliptic flow appears to track the shear viscosity of the preceding QGP phase: lower values of $(\eta/s)_{QGP}$ produce lower values of $(\eta/s)(T)$ below T_c , and *vice versa*. Clearly, the extracted hadronic $(\eta/s)(T)$ is not an intrinsic medium property of the hadron resonance gas in **UrQMD**, but a parameter that preserves some memory of the QGP transport properties (in fact, only of the transport properties at temperatures just above T_{chem} , see Fig. 11).

Through a sequence of cross-checks we convinced ourselves that our method to extract an effective $(\eta/s)(T)$ for the hadronic matter in **UrQMD** failed because in **UrQMD** the viscous corrections in the energy-momentum tensor relax to their Navier-Stokes values much more slowly than assumed in **VISH2+1**. As a consequence, the extracted η/s fitted the value of the viscous pressure tensor $\pi^{\mu\nu}$ inherited by **UrQMD** from **VISH2+1** (and thus characterized by

the η/s value in the preceding QGP phase) instead of the shear viscosity characteristic of **UrQMD** matter.

An independent extraction of both the relaxation time τ_π and the shear viscosity from **UrQMD** is presently beyond our technical means. Our results suggest that it may be possible to achieve a good emulation of **UrQMD** dynamics with viscous hydrodynamics, by using **VISH2+1** with larger specific shear viscosities η/s combined with larger relaxation times τ_π in the hadronic phase than those assumed in the present work (which were constrained by the relation $T\tau_\pi = 3\eta/s$). We are skeptic, however, about the prospects for finding a pair of functions $(\eta/s)(T)$ and $T\tau_\pi(T)$ that work universally, *i.e.* that yield good viscous hydrodynamic emulations of **UrQMD** independent of the initial input into **UrQMD** (in particular, independent of the initial values of the viscous terms in $T^{\mu\nu}$ that are to be further evolved with **UrQMD**). The reason for our skepticism is that large relaxation times τ_π indicate a fundamental breakdown of the viscous hydrodynamic framework: They appear as second-order corrections to ideal fluid dynamics in a systematic gradient expansion, and if they lead to large excursions of the viscous pressure $\pi^{\mu\nu}$ away from its first-order Navier-Stokes value $\pi^{\mu\nu} = 2\eta\sigma^{\mu\nu}$, this indicates that the gradient expansion is no longer converging.

With this state of present knowledge we conclude that there exists no “switching window” of temperatures below T_{chem} for safely switching from **VISH2+1** to **UrQMD**, *i.e.* there is no temperature interval below T_{chem} in which **VISH2+1** and **UrQMD** can both be used equally well to describe the evolution of the expanding medium created in relativistic heavy-ion collisions. Quantitative comparisons with experimental data, with the goal of extracting from measured hadron spectra precise information of QGP transport properties, will therefore necessarily require the use of a hybrid code like **VISHNU** in which the dynamics of the late hadronic stage (at all temperatures below T_{chem}) is described microscopically.

ACKNOWLEDGMENTS

We gratefully acknowledge fruitful discussions with V. Koch and T. Hirano, whom we also thank for providing the averaged initial density profiles for fluctuating CGC initial conditions. We thank P. Huovinen for sending us the EOS s95p-PCE before publication and T. Riley and C. Shen for providing a fit function [25] for this EOS and implementing it into **VISH2+1**. This work was supported by the U.S. Department of Energy under contracts DE-AC02-05CH11231, DE-FG02-05ER41367, DE-SC0004286, and (within the framework of the Jet Collaboration) DE-SC0004104. We gratefully acknowledge extensive computing resources provided to us by the Ohio Supercomputer Center.

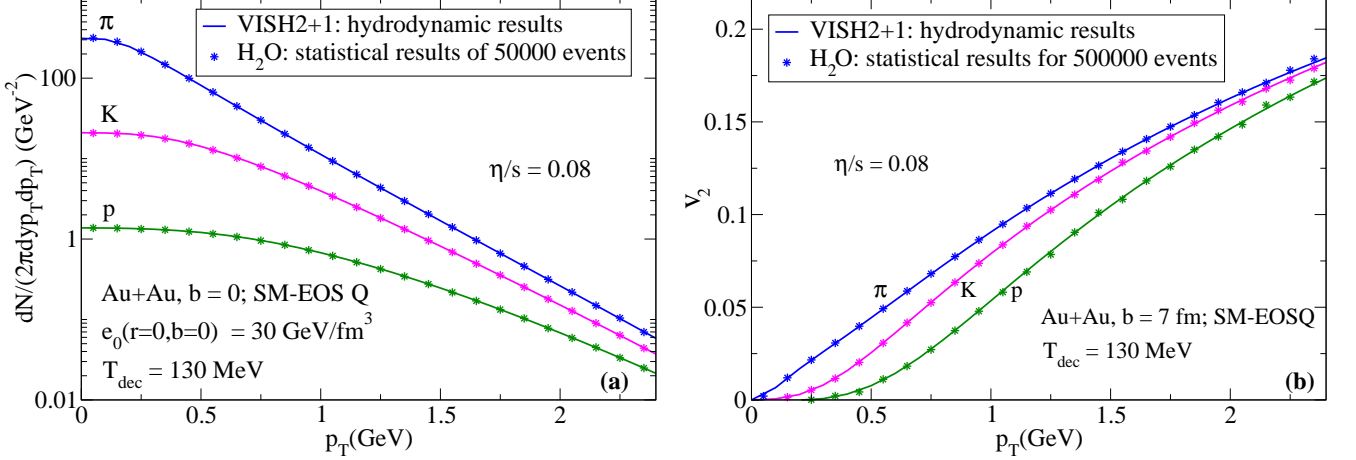


FIG. 12. (Color online) p_T spectra for central Au+Au collisions and $v_2(p_T)$ for non-central Au+Au collisions at $b=7$ fm, from VISH2+1 and H₂O.

Appendix A: Verification of the VISH2+1 to UrQMD converter

In VISHNU the connection between VISH2+1 and UrQMD is realized by the Monte-Carlo particle generator H₂O, which is briefly described in Sec. II B. This appendix details the verification of H₂O against the analytical Cooper-Frye formula on which it is based.

H₂O randomly generates an ensemble of particles in momentum and position space based on the differential Cooper-Frye formula, Eq. (1), for each collision event, which can subsequently be used as initial configuration for UrQMD. Here, we directly perform a statistical analysis of sufficiently many such initial configurations obtained from H₂O to generate smooth particle spectra and elliptic flow curves, which we then compare to a direct numerical integration of Eq. (1) along the freeze-out surface generated by VISH2+1.

Figure 12 shows p_T -spectra for pions, protons and kaons in central (a) and their differential $v_2(p_T)$ in non-central (b) Au+Au collisions, obtained from VISH2+1 directly and via H₂O, respectively. To specifically test the “viscous part” of the H₂O event generator, we select a constant specific shear viscosity $\eta/s = 0.08$. With a sufficiently large number of events, the statistical results from H₂O exactly reproduce the hydrodynamic spectra and v_2 directly obtained from VISH2+1.

The above hadron spectra are generated on a decoupling hypersurface with $T_{\text{dec}} = 130$ MeV.¹³ In Fig. 13, we show the 2-dimensional r - τ freeze-out hypersurface for central Au+Au collisions. The black line is the hydrodynamic freeze-out hypersurface obtained from VISH2+1, and the red symbols are the pion emission points taken from a single H₂O event, all of which fall on the VISH2+1

freeze-out hypersurface. The small deviations which can be seen are due to the finite position resolution in H₂O, which randomly samples particle positions on the freeze-out hypersurface within $\Delta r = 0.1$ fm. Fig. 13 also shows that only few particles come from the very early stage of the fireball evolution, while most of the particles are emitted during the middle and late stages when the flow velocity is fully developed. This is illustrated in the inset of Fig. 13, which shows the emission rate for pions as a function of time (along the freeze-out hypersurface). Again the statistical results from H₂O are in excellent agreement with the hydrodynamic results from VISH2+1 showing that H₂O correctly reproduces the particle emission rates of VISH2+1 along the freeze-out hypersurface.

Momenta and positions of the produced particles are correlated through Eq. (1). For example, the equilibrium

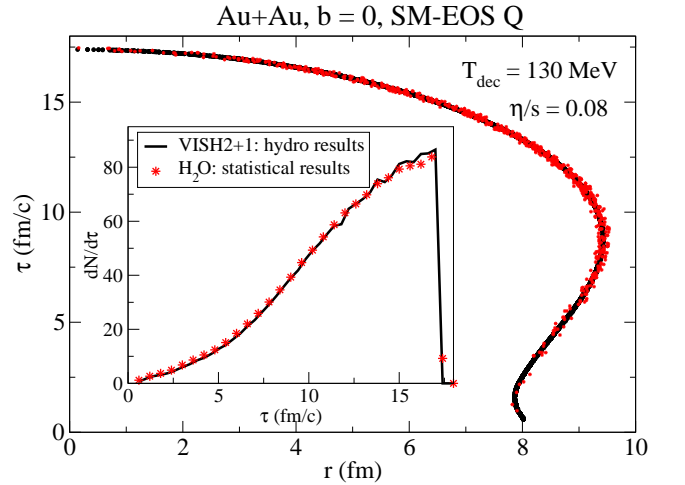


FIG. 13. (Color online) VISH2+1: hydrodynamic freeze-out surface for central ($b=0$) Au+Au collisions with decoupling temperature $T_{\text{dec}} = 130$ MeV. H₂O: pion emission points along the freeze-out surface from a single event. Inset: pion emission rate along the freeze-out surface.

¹³ We here selected the “default” $T_{\text{dec}} = 130$ MeV for EOS-Q, but the quality of the code verification results does not depend on the chosen decoupling/switching temperature.

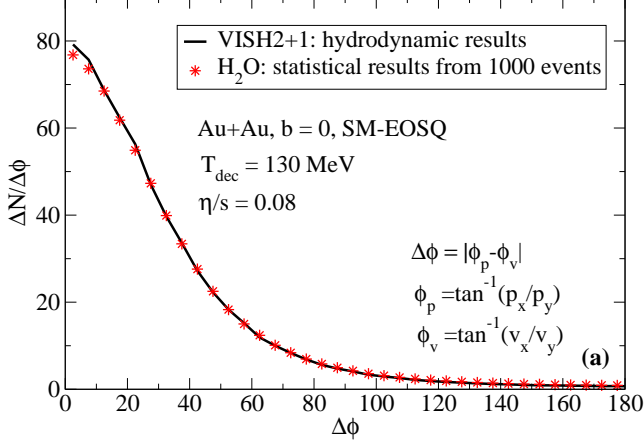


FIG. 14. (Color online) Left: Pion emission probabilities as a function of emission angle $\Delta\phi = |\phi_p - \phi_v|$ from VISH2+1 and H₂O.

distribution f for $\mu = 0$ can be explicitly written as

$$f_{\text{eq}} = \frac{1}{e^{\gamma_{\perp} [m_T \cosh(y - \eta_s) - p_T v_{\perp} \cos(\phi_p - \phi_v)] / T} \pm 1}. \quad (\text{A1})$$

This shows directly the correlation between the transverse flow velocity v_{\perp} and transverse momentum p_T of the particles, as well as the correlation between momentum rapidity y and space rapidity η_s . (Here $\phi_p = \arctan(p_x/p_y)$ is the angle of the particle transverse momentum and $\phi_v = \arctan(v_x/v_y)$ is the angle of the transverse flow velocity.)

In fact, the above form of the distribution function leads to enhanced particle production along the flow velocity direction, but suppresses particle production in the opposite direction. This is shown in Fig. 14 which shows the particle production rate as a function of the relative emission angle $\Delta\phi = |\phi_p - \phi_v|$. Both the hydrodynamic result from VISH2+1 as well as the statistical result from H₂O show that $\Delta N/\Delta\phi$ reaches a peak when $\Delta\phi$ is zero (particle emission along the flow velocity direction), then rapidly decreases with increasing $\Delta\phi$, and reaches a minimum for $\Delta\phi = 180^\circ$. The excellent agreement between the VISH2+1 and H₂O results show that H₂O correctly describes the particle momentum and flow velocity correlations encoded in Eq. (1).

The Bjorken approximation in (2+1)-dimensional viscous hydrodynamics leads to a uniform particle density

as a function of momentum-space rapidity and likewise a uniform particle density as a function of space-time rapidity. Eq. (1) (together with Eq. (A1)) shows the correlation between momentum-space and space-time rapidity, which prevents H₂O from generating particles with independent momentum-space and space-time rapidities. In practice, H₂O first randomly generates the momentum-space rapidity y for each hadron within a finite predefined range (for example between -3 and +3) and then samples the space-time rapidity η_s through Eq. (1). The finite range of y , together with the $y - \eta_s$ correlation, leads to a decrease of $dN/d\eta_s$ in the boundary region of η_s as shown in the inset of Fig. 15.

Fig. 15 shows the correlation between y and η_s for pions. In excess of 90% of pions are produced at a space-time rapidity which lies within one unit of its momentum-space rapidity. In other words, most of the particles with forward (backward) momentum-space rapidity are generated in forward (backward) space-time rapidity regions. Fig. 15 also shows that the hydrodynamic results from VISH2+1 and statistical results from H₂O agree very well with each other, indicating that H₂O correctly describes the momentum-space and space-time rapidity correlation in particle production.

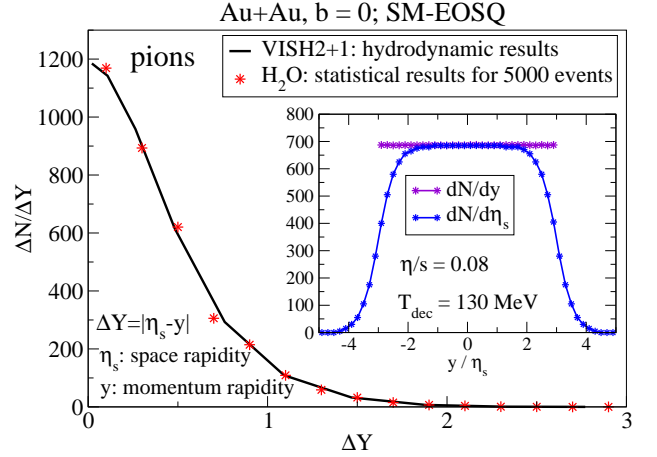


FIG. 15. (Color online) Left: Pion emission probabilities as a function of emission rapidity $\Delta Y = |\eta_s - y|$ for VISH2+1 and H₂O. Inset: Pion production as a function of momentum rapidity y and space-time rapidity η_s , from H₂O.

- [1] U. Heinz and P. F. Kolb, Nucl. Phys. A **702**, 269 (2002).
- [2] P. F. Kolb and U. Heinz, in *Quark-Gluon Plasma 3*, edited by R. C. Hwa and X.-N. Wang (World Scientific, Singapore, 2004), p. 634 [arXiv:nucl-th/0305084];
- [3] M. Gyulassy, in *Structure and dynamics of elementary matter*, edited by W. Greiner *et al.*, NATO science series II: Mathematics, physics and chemistry, Vol. 166 (Kluwer

- Academic, Dordrecht, 2004), p. 159-182 [arXiv:nucl-th/0403032].
- [4] M. Gyulassy and L. McLerran, Nucl. Phys. **A750**, 30 (2005); E. V. Shuryak, *ibid.*, p. 64.
- [5] I. Arsene *et al.* (BRAHMS Collaboration), Nucl. Phys. **A757**, 1 (2005); B. B. Back *et al.* (PHOBOS Collaboration), *ibid.*, p. 28; J. Adams *et al.* (STAR Collaboration),

- ibid.*, p. 102; K. Adcox *et al.* (PHENIX Collaboration), *ibid.*, p. 184.
- [6] P. Danielewicz, M. Gyulassy, Phys. Rev. D **31**, 53 (1985).
- [7] G. Policastro, D. T. Son and A. O. Starinets, Phys. Rev. Lett. **87**, 081601 (2001); P. K. Kovtun, D. T. Son and A. O. Starinets, Phys. Rev. Lett. **94**, 111601 (2005).
- [8] D. Teaney, Phys. Rev. C **68**, 034913 (2003); R. A. Lacey and A. Taranenko, PoS **CFRNC2006**, 021 (2006); R. A. Lacey *et al.*, Phys. Rev. Lett. **98**, 092301 (2007); A. Adare *et al.*, Phys. Rev. Lett. **98**, 172301 (2007); H.-J. Drescher, A. Dumitru, C. Gombeaud, and J.-Y. Ollitrault, Phys. Rev. C **76**, 024905 (2007). K. Dusling and D. Teaney, Phys. Rev. C **77**, 034905 (2008); Z. Xu, C. Greiner, and H. Stöcker, Phys. Rev. Lett. **101**, 082302 (2008); D. Molnar and P. Huovinen, J. Phys. G **35**, 104125 (2008); R. A. Lacey, A. Taranenko and R. Wei, in *Proc. 25th Winter Workshop on Nuclear Dynamics*, W. Bauer, R. Bellwied, and J.W. Harris (eds.), (EP Systema, Budapest, 2009) p. 73 [arXiv:0905.4368]; K. Dusling, G. D. Moore, and D. Teaney, Phys. Rev. C **81**, 034907 (2010); A. K. Chaudhuri, J. Phys. G **37**, 075011 (2010); R. A. Lacey *et al.*, Phys. Rev. C **82**, 034910 (2010).
- [9] P. Romatschke and U. Romatschke, Phys. Rev. Lett. **99**, 172301 (2007); M. Luzum and P. Romatschke, Phys. Rev. C **78**, 034915 (2008).
- [10] H. Song and U. Heinz, Phys. Lett. **B658**, 279 (2008); Phys. Rev. C **77**, 064901 (2008); **78**, 024902 (2008); H. Song, Ph.D Thesis, The Ohio State University (August 2009), arXiv:0908.3656 [nucl-th].
- [11] H. Song and U. Heinz, J. Phys. G **36**, 064033 (2009).
- [12] H. Song, S. A. Bass, U. Heinz, T. Hirano and C. Shen, arXiv:1011.2783 [nucl-th]; and to be published.
- [13] D. Molnar, M. Gyulassy, Nucl. Phys. **A697**, 495 (2002).
- [14] F. Cooper and G. Frye, Phys. Rev. D **10**, 186 (1974).
- [15] J. Aichelin and H. Stöcker, Phys. Lett. B **176**, 14 (1986); H. Stöcker and W. Greiner, Phys. Rept. **137** (1986) 277; H. Sorge, H. Stöcker and W. Greiner, Ann. Phys. (N.Y.) **192**, 266 (1989).
- [16] T. Maruyama, W. Cassing, U. Mosel, S. Teis and K. Weber, Nucl. Phys. A **573**, 653 (1994); W. Ehehalt and W. Cassing, Nucl. Phys. A **602**, 449 (1996).
- [17] X. S. Fang, C. M. Ko, G. Q. Li and Y. M. Zheng, Nucl. Phys. A **575**, 766 (1994); B. Zhang, C. M. Ko, B. A. Li and Z. w. Lin, Phys. Rev. C **61**, 067901 (2000).
- [18] S. A. Bass *et al.*, Prog. Part. Nucl. Phys. **41**, 255 (1998); M. Bleicher *et al.*, J. Phys. G **25**, 1859 (1999).
- [19] Y. Nara, N. Otuka, A. Ohnishi, K. Niita and S. Chiba, Phys. Rev. C **61**, 024901 (2000).
- [20] S. A. Bass and A. Dumitru, Phys. Rev. **C61**, 064909 (2000).
- [21] D. Teaney, J. Lauret and E. V. Shuryak, Phys. Rev. Lett. **86**, 4783 (2001); arXiv:nucl-th/0110037; and Nucl. Phys. A **698**, 479 (2002).
- [22] T. Hirano, U. Heinz, D. Kharzeev, R. Lacey and Y. Nara, Phys. Lett. B **636**, 299 (2006).
- [23] C. Nonaka and S. A. Bass, Phys. Rev. C **75**, 014902 (2007).
- [24] P. Huovinen and P. Petreczky, Nucl. Phys. A **837**, 26 (2010).
- [25] C. Shen, U. Heinz, P. Huovinen and H. Song, Phys. Rev. C **82**, 054904 (2010).
- [26] A. Bazavov *et al.*, Phys. Rev. D **80**, 014504 (2009).
- [27] S. Borsanyi *et al.*, arXiv:1011.4229 [hep-lat] and arXiv:1011.4230 [hep-lat]; S. Borsanyi *et al.* [Wuppertal-Budapest Collaboration], JHEP **1009**, 073 (2010), and JHEP **1011**, 077 (2010).
- [28] P. Braun-Munzinger, D. Magestro, K. Redlich and J. Stachel, Phys. Lett. **B518** (2001) 41; J. Adams *et al.* [STAR Collaboration], Nucl. Phys. **A757** (2005) 102; A. Andronic, P. Braun-Munzinger and J. Stachel, Phys. Lett. **B673** (2009) 142 [Erratum-*ibid.* **B678** (2009) 516].
- [29] S. A. Bass *et al.*, Phys. Rev. C **60**, 021902 (1999).
- [30] L. V. Bravina *et al.*, Phys. Lett. **B434**, 379-387 (1998).
- [31] D. Teaney, arXiv:nucl-th/0204023;
- [32] T. Hirano and K. Tsuda, Phys. Rev. C **66**, 054905 (2002);
- [33] P. F. Kolb and R. Rapp, Phys. Rev. C **67**, 044903 (2003);
- [34] P. Huovinen, Eur. Phys. J. A **37**, 121 (2008).
- [35] T. Hirano and M. Gyulassy, Nucl. Phys. A **769**, 71 (2006).
- [36] H. Song and U. Heinz, Nucl. Phys. A **830**, 467C (2009); and Phys. Rev. C **81**, 024905 (2010).
- [37] G. S. Denicol, T. Kodama and T. Koide, J. Phys. G **37**, 094040 (2010).
- [38] P. Bozek, Phys. Rev. C **81**, 034909 (2010).
- [39] P. B. Arnold, G. D. Moore and L. G. Yaffe, JHEP **0305**, 051 (2003).
- [40] H. J. Drescher and Y. Nara, Phys. Rev. C **75**, 034905 (2007); **76**, 041903(R) (2007).
- [41] T. Hirano and Y. Nara, Phys. Rev. C **79**, 064904 (2009); and Nucl. Phys. **A830**, 191c (2009).
- [42] R. Baier, P. Romatschke and U. A. Wiedemann, Phys. Rev. C **73**, 064903 (2006).
- [43] M. Belkacem *et al.*, Phys. Rev. C **58**, 1727 (1998).
- [44] L. V. Bravina, E. E. Zabrodin, S. A. Bass *et al.*, Phys. Rev. C **63**, 064902 (2001).
- [45] N. Demir and S. A. Bass, Phys. Rev. Lett. **102**, 172302 (2009); N. Demir and S. A. Bass, Nucl. Phys. **A830**, 733c (2009).
- [46] K. Werner *et al.*, J. Phys. G **36**, 064030 (2009); and Phys. Rev. C **82**, 044904 (2010).
- [47] T. Hirano, U. Heinz, D. Kharzeev, R. Lacey and Y. Nara, Phys. Rev. C **77**, 044909 (2008).
- [48] P. F. Kolb, J. Sollfrank and U. Heinz, Phys. Lett. B **459**, 667 (1999); and Phys. Rev. C **62**, 054909 (2000).
- [49] G. D. Moore and O. Saremi, JHEP **0809**, 015 (2008); M. A. York and G. D. Moore, Phys. Rev. D **79**, 054011 (2009).
- [50] L. P. Csernai, J. I. Kapusta and L. D. McLerran, Phys. Rev. Lett. **97**, 152303 (2006).
- [51] J. W. Chen, M. Huang, Y. H. Li, E. Nakano and D. L. Yang, Phys. Lett. B **670**, 18 (2008).
- [52] J. I. Kapusta, arXiv:0809.3746 [nucl-th].
- [53] C. M. Hung and E. V. Shuryak, Phys. Rev. C **57**, 1891 (1998).
- [54] N. Demir and S.A. Bass, unpublished notes.
- [55] W. Israel, Ann. Phys. (N.Y.) **100**, 310 (1976); W. Israel and J. M. Stewart, *ibid.* **118**, 341 (1979).